Effect of turbulent fluctuations of refractive index on the time spectrum of wind velocity measured by Doppler lidar

V.A. Banakh, Ch. Werner, and I.N. Smalikho

Institute of Atmospheric Optics,
Siberian Branch of the Russian Academy of Sciences, Tomsk, Russia
Institute of Atmospheric Physics,
German Aerospace Center, Oberpfaffenhofen, Germany

Received May 3, 2000

The effect of turbulent fluctuations of the air refractive index in the atmosphere on the time spectrum of wind velocity measured by a cw Doppler CO_2 lidar is studied by numerical simulation. It is shown that fluctuations of the refractive index can cause considerable random displacements of the laser beam focusing area determining an effective sounded volume along the beam propagation axis. The correlation time of these displacements is roughly equal to the time of transfer of medium inhomogeneities by a cross wind to the distance equal to the initial radius of the sounding beam. Random displacements of the sounded volume can just cause the experimentally observed essential increase in the energy of fluctuations in the high-frequency range of the turbulent spectrum of wind velocity measured by the lidar.

Introduction

An effect of spatial averaging over a sounded volume on the accuracy of the mean wind velocity measured by a cw Doppler CO_2 lidar was studied in detail in Refs. 1–3. It was proposed that for the wavelength $\lambda = 10.6$ μm, relatively short sounding paths (up to 1 km), and the structure characteristic of fluctuations of the refractive index in the surface atmospheric layer $C_n^2 \lesssim 10^{-12}$ m$^{-2/3}$, we can neglect the effect of random variations of the refractive index. However, experiments show that for a large sounded volume the time spectra of velocity measured by a lidar in some cases differ essentially from theoretical dependences.[3] In this paper, the effect of turbulent fluctuations of the air refractive index on the time spectrum of wind velocity measured by a lidar is studied by numerical simulation.

1. Formulation of the problem

The velocity V_D measured by a cw Doppler lidar at the time t can be presented as[3]

$$V_D(t) = \int_0^\infty dz\, V_r(z, t)\, Q_s(z, t) + V_e(t), \qquad (1)$$

where $V_r(z, t)$ is the radial component of wind velocity at the point spaced by z from the lidar in the propagation direction of a laser beam;

$$Q_s(z, t) = \mu_s(z, t) \Big/ \int_0^\infty dz\, \mu_s(z, t) \qquad (2)$$

is the function characterizing the spatial resolution;

$$\mu_s(z, t) = t_0^{-1} \int_{t-t_0}^{t} dt' \int d^2\rho\, I^2(z, \rho, t'); \qquad (3)$$

t_0 is the integral time for measurement of one Doppler power spectrum of the lidar return signal; $I(z, \rho, t')$ is the instantaneous intensity distribution of the sounding beam in the plane $\rho = \{x, y\}$ normal to the propagation axis z; $V_e(t)$ is the random error of estimation of the radial wind velocity averaged over the sounded volume due to fluctuations of a lidar return signal and noise of a measurement system. For the considered case of long integral time $t_0 \sim 50$ μs and large dimensions of the sounded volume, we can consider the lidar return signal statistics as Gaussian one[4] and neglect the error V_e. Therefore, henceforth we assume $V_e = 0$ in Eq. (1). In contradistinction to Ref. 3, Eqs. (1)–(3) allow us to take into account variations of Q_s in time due to turbulent variations of the air refractive index at the sounding path.

In the absence of turbulence ($C_n^2 = 0$), the sounding beam intensity is determined by the equation[3]

$$I(z, \rho) = \frac{P_T}{\pi a_0^2\, g^2(z)} \exp\left\{-\frac{\rho^2}{a_0^2\, g^2(z)}\right\}, \qquad (4)$$

where $g^2(z) = (1 - z/R)^2 + (z/ka_0^2)^2$, $k = 2\pi/\lambda$; P_T is the power; R is the focal length; and a_0 is the initial radius of the sounding beam. Correspondingly, at $C_n^2 = 0$ for the function $Q_s(z, t) \equiv Q_s(z)$ and its maximum z_{max} lying at the axis z, we have from Eqs. (2)–(4)

$$Q_s(z) = \left\{g^2(z)\, ka_0^2 \left[\frac{\pi}{2} + \arctan\left(\frac{ka_0^2}{R}\right)\right]\right\}^{-1}, \qquad (5)$$

$$z_{max} = R/[1 + (R/ka_0^2)^2]. \qquad (6)$$

0235-6880/00/09 741-06 $02.00

For the length of the sounded volume determined as $\Delta z = Q_s^{-1}(z_{max})$, from Eqs. (5) and (6) we have

$$\Delta z = \frac{R^2}{ka_0^2} \frac{\pi/2 + \arctan(ka_0^2/R)}{1 + (R/ka_0^2)^2}. \qquad (7)$$

Under the condition $ka_0^2 \gg R$, the function $Q_s(z)$ is practically symmetric about the point $z = z_{max}$, and $z_{max} \approx R$ is the distance from the lidar to the center of the sounded volume, whereas the length of the sounded volume, as follows from Eq. (7), has the square dependence on R (Refs. 1–5):

$$\Delta z \approx (\lambda/2)(R/a_0)^2.$$

It is shown in Ref. 1 that as Δz is large enough and the hypothesis of "frozen" turbulence[6,7] is valid, the time spectrum of velocity measured by a lidar $S_D(f) = 2\int_{-\infty}^{+\infty} d\tau \langle V_D(t+\tau)\, V_D(t)\rangle\, e^{-2\pi j f\tau}$ in the inertial range of turbulence has the form

$$S_D(f) = 0.06\varepsilon^{2/3} U^{5/3} \Delta z^{-1} f^{-8/3}, \qquad (8)$$

where ε is the dissipation rate of turbulent energy; U is the wind velocity component transverse to the direction of sounding. In many cases, experimental results actually correspond to the "$-8/3$" power dependence of the spectrum on frequency, and the values of the dissipation rate ε estimated from measured spectra are quite acceptable. However, in some cases the measured spectra S_D have significant deviations from the frequency dependence (8) even when the hypothesis of frozen turbulence is fulfilled undoubtedly. To reveal the cause of such deviations, $Q_s(z, t)$ was studied as a function of C_n^2 by simulating numerically the propagation of the focused sounding beam with the parameters $\lambda = 10.6$ μm and $a_0 = 7.5$ cm through the turbulent atmosphere. Then numerical simulation of random realizations of the radial wind velocity $V_r(z, t)$, along with the hypothesis of frozen turbulence for $V_r(z, t)$ and $I(z, \rho, t)$, was used to calculate the time spectra $S_D(f)$ for the integral time $t_0 = 50$ μs (t_0^{-1} is the data reading frequency) and different C_n^2, U, and R.

2. Results of numerical simulation

For numerical simulation of random realizations of the intensity $I(z, \rho, t)$ of the focused beam propagating through the turbulent atmosphere, we used the method of phase screens.[8] The path of length $L = 2R$ was divided into 100 layers having equal thickness ΔR. The phase $\psi(\Delta Ri, \rho, t)$ and intensity $I(\Delta Ri, \rho, t)$, where i is the layer number, were simulated at the nodes of a uniform grid $\rho = \{\Delta xm, \Delta yl\}$. The intensity $I(\Delta Ri, \rho, t)$ as a function of time t was obtained by displacing the grid of simulated phase values $\psi(\Delta Ri, \rho, t)$ by $\Delta x = U\Delta t$, where the interval Δt was taken so that it was much smaller than the correlation time of the intensity of the propagating beam. Then the function $Q_s(z, t)$ was calculated from $n = t_0/\Delta t$ values of the intensity obtained sequentially by Eqs. (2) and (3).

2.1. Statistics of parameters of sounding volume

The function $Q_s(z, t)$ was simulated without averaging over the integral time t_0, so we assumed $t_0 \to 0$ in Eq. (3).

Figure 1 exemplify simulation of random realizations of $Q_s(z, t)$ for $t_0 \to 0$ (solid curves) for the parameters $R = 500$ m, $C_n^2 = 10^{-13}$ m$^{-2/3}$ (*a*) and $C_n^2 = 10^{-12}$ m$^{-2/3}$ (*b*). The function $Q_s(z, t)$ calculated by Eq. (5) for $C_n^2 = 0$ is shown as a dashed curve. One can see that for $C_n^2 = 10^{-13}$ m$^{-2/3}$ the fluctuations of the refractive index cause only random displacements of the center of the sounded volume z_{max} along the optical axis and keep the shape of the curves practically unchanged. For $C_n^2 = 10^{-12}$ m$^{-2/3}$, besides random displacements of the sounded volume Δz, its length increases considerably.

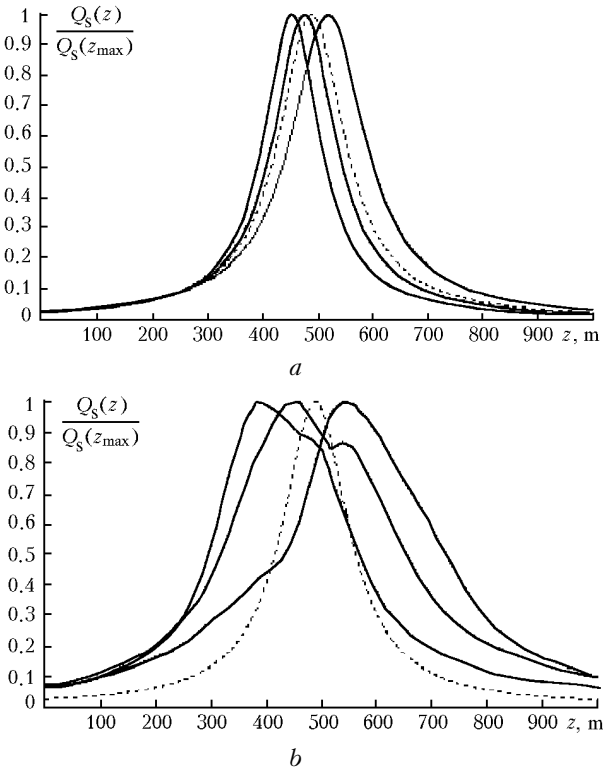

Fig. 1. Examples of simulation of random realizations of the function $Q_s(z, t)$ for $C_n^2 = 10^{-13}$ m$^{-2/3}$ (*a*) and $C_n^2 = 10^{-12}$ m$^{-2/3}$ (*b*) (solid curves); calculation by Eq. (5) (dashed curve).

From the obtained random realizations of $Q_s(z, t)$ the following characteristics were calculated: the variance $\sigma_z^2 = \langle z'^2_{max}\rangle$, the coefficient of time correlation between displacements of the center of the sounded volume $K_z(\tau) = \langle z'_{max}(t+\tau)\, z'_{max}(t)\rangle/\sigma_z^2$, where $z'_{max} = z_{max} - \langle z_{max}\rangle$, and its average dimension $\Delta z = \langle Q_z^{-1}(z_{max})\rangle$.

Points in Figs. 2 and 3 show the calculated results on the mean square deviation σ_z as a function of C_n^2 and R. Solid curves show the dependences $\sigma_z^2 \sim C_n^2$ and $\sigma_z \sim R^2$. It follows therefrom that the mean square deviation of displacements σ_z and the length of the sounded volume $\Delta z = \Delta z_0$ for $C_n^2 = 0$ (see Eq. (7) for $ka_0^2 \gg R$) are proportional to R^2. Correspondingly, the ratio $\Delta z_0/\sigma_z$ is practically independent of the sounding range R, at least, within 250 m $\le R \le$ 1 km.

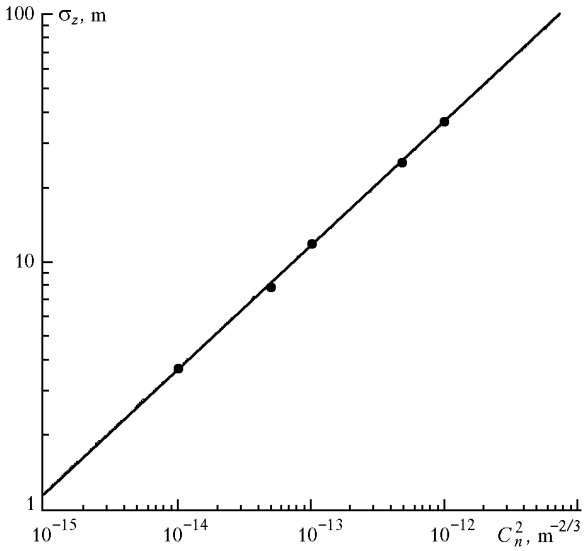

Fig. 2. Mean square deviation of displacements of sounded volume σ_z as a function of C_n^2 for R = 500 m.

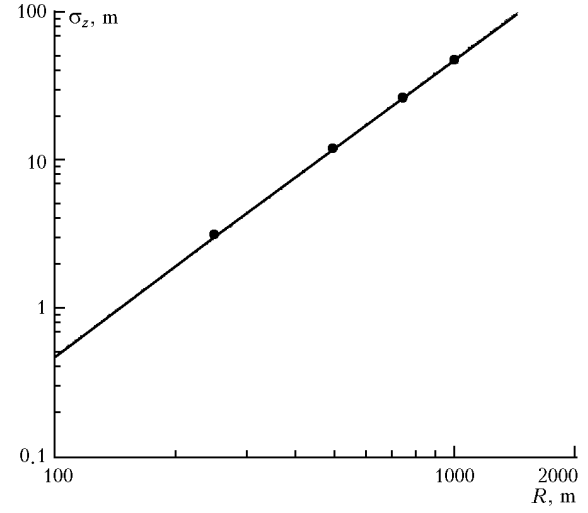

Fig. 3. Mean square deviation of displacements of sounded volume σ_z as a function of R for $C_n^2 = 10^{-13}$ m$^{-2/3}$.

Figure 4 shows the dependence of Δz on C_n^2 for R = 500 m as points. The solid horizontal line corresponds to $\Delta z = \Delta z_0$ in the absence of turbulence. It is seen that Δz differs a little from Δz_0 up to $C_n^2 = 10^{-13}$ m$^{-2/3}$, and for $C_n^2 = 10^{-12}$ m$^{-2/3}$ it increases almost 1.5 times.

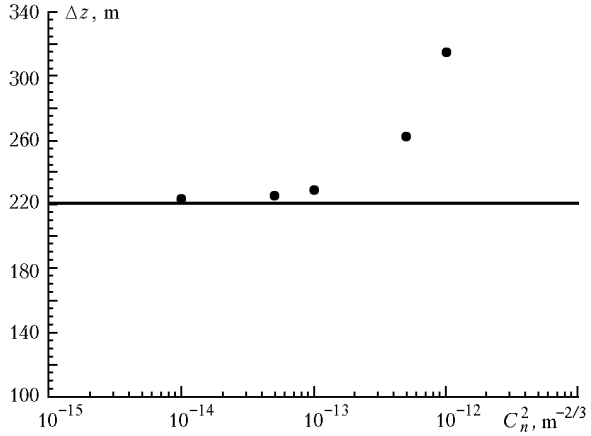

Fig. 4. Mean length of sounded volume Δz vs. C_n^2 for R = 500 m.

Figure 5 shows the coefficient of time correlation between displacements of the sounded volume due to turbulent fluctuations of the refractive index for R = 500 m and $C_n^2 = 10^{-13}$ m$^{-2/3}$. The analogous dependences for $K_z(\tau)$ were obtained for other R and C_n^2 as well. It follows from analysis of the calculated results on $K_z(\tau)$ that the correlation time between displacements of the sounded volume τ_z is determined by the time of transfer of turbulent inhomogeneities of the refractive index with the mean wind velocity U to the distance equal to the initial beam radius a_0 ($\tau_c \approx a_0/U$). For example, for a_0 = 7.5 cm and U = 4 m/s the correlation time is $\tau_z \approx$ 0.02 s. It is well known[9] that in the atmospheric boundary layer the correlation time of wind velocity fluctuations is $\tau_V \sim$ 10–20 s. Therefore, τ_V exceeds τ_z approximately by a factor of 10^3. So, to simulate $V_D(t)$ based on Eqs. (1)–(3), we have to have the array of $\int d^2\rho\, I^2(z, \rho, t)$ values which approximately 10^3 times exceeds the array of $V_r(z, t)$ values. Such large computational volume restricts severely the possibility of implementing the algorithm of direct simulation for $V_D(t)$ and forces the use of approximate methods.

As is seen from Fig. 1*a*, the shape of instantaneous ($t_0 \to 0$) distributions $Q_s(z, t)$ for $C_n^2 = 10^{-13}$ m$^{-2/3}$ differs a little from $Q_s(z)$ calculated for $C_n^2 = 0$ (see the dashed curve) for different $R = \tilde{R}(t)$. So, for the function $Q_s(z, t)$ we can use the approximation based on representation of the instantaneous intensity distribution $I(z, \rho, t)$ in Eq. (3), by analogy with Eq. (4), as

$$I(z, \rho, t) = \frac{P_T}{\pi a_0^2 \tilde{g}^2(z, t)} \exp\left\{-\frac{\rho^2}{a_0^2 \tilde{g}^2(z, t)}\right\}, \quad (9)$$

where

$$\tilde{g}^2(z, t) = [1 - z/\tilde{R}(t)]^2 + (z/ka_0^2)^2. \quad (10)$$

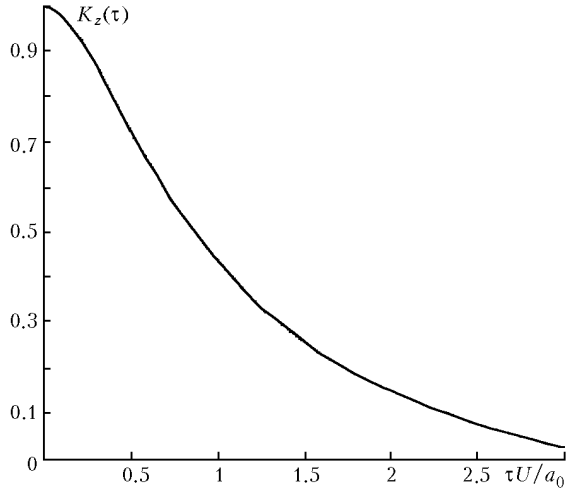

Fig. 5. Coefficient of time correlation of displacements of sounded volume due to refraction turbulence.

Upon substitution of Eq. (9) into Eqs. (3) and (2) and integration over ρ and z, for $Q_s(z, t)$ we obtain

$$Q_s(z, t) = \frac{t_0^{-1} \int\limits_{t-t_0}^{t} dt' \, \tilde{g}^{-2}(z, t')}{ka_0^2 \left\{ \frac{\pi}{2} + \int\limits_{t-t_0}^{t} dt' \arctan [ka_0^2/\tilde{R}(t')] \right\}} . \quad (11)$$

From Eq. (11) it is easy to find the relation between $\tilde{R}(t)$ and $z_{max}(t)$ at $t_0 \to 0$:

$$\tilde{R}(t) = \frac{1}{2} ka_0^2 \left[\frac{ka_0^2}{z_{max}(t)} - \sqrt{\left[\frac{ka_0^2}{z_{max}(t)} \right]^2 - 4} \right] . \quad (12)$$

The comparison of the functions $Q_s(z, t)$ simulated directly [by substituting the random intensity distribution $I(z, \rho, t)$ into Eqs. (3) and (2)] and those obtained with the use of the corresponding values of $z_{max}(t)$ in Eqs. (12) and (11) shows that their difference is small up to $C_n^2 \lesssim 10^{-13}$ m$^{-2/3}$. In the case of large C_n^2 (for example, $C_n^2 = 10^{-12}$ m$^{-2/3}$), the use of the approximation (11)–(12) becomes impossible because of the essential increase in the length of the sounded volume (see Figs. 1*b* and 4).

Thus, the problem of determination of $Q_s(z, t)$ reduces to simulation of the time dependence of displacements of the sounded volume $z_{max}(t)$, where $t \in [0, T]$. In this case, the time interval T and the data sampling frequency Δt^{-1} must satisfy the conditions: $T \gg \tau_V$ and $\Delta t \ll \tau_z$.

From two simulated discrete sequences $z_{max}(i\Delta t)$, where $i = 1, 2, \ldots, 512$, with $\Delta t = \Delta x/U$ and $\Delta t = a_0/U$ ($a_0/\Delta x = 15$) we obtained two estimates for the power spectrum of displacements of the sounded volume $S_z(f) = \sigma_z^2 \int\limits_{-\infty}^{+\infty} d\tau \, K_z(\tau) \, e^{-2\pi j f \tau}$. In this case, moving smoothing by a rectangular spectral window including nine spectral frequencies was used. The estimation error for such spectra is approximately 30%. Figure 6 shows the obtained spectra as solid curves *1* ($\Delta t = \Delta x/U$) and *2* ($\Delta t = a_0/U$). Based on these data, the approximation formula was chosen for the spectrum $S_z(f)$ as

$$S_z(f) = \sigma_z^2 \frac{2\tau_z}{[1 + (4.48\tau_z f)^2]^{4/3}} , \quad (13)$$

where $\tau_z = a_0/U$ is the integral correlation scale for displacements of the sounded volume $\tau_z = \int\limits_0^{\infty} dz \, K_z(\tau)$. Calculation by Eq. (13) is shown in Fig. 6 as a dashed curve.

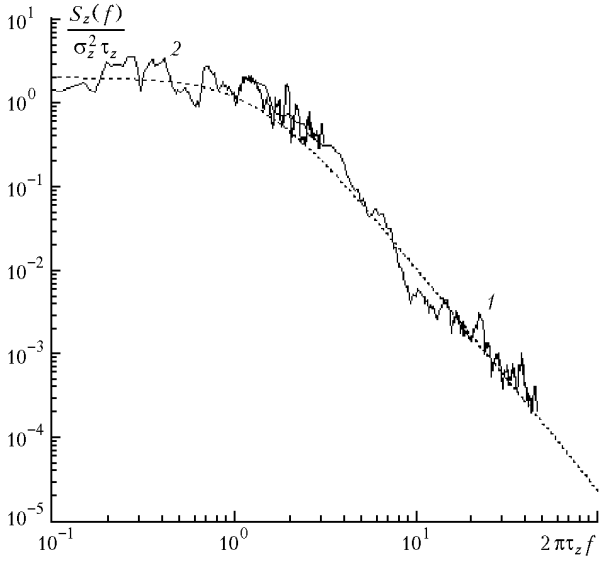

Fig. 6. Time spectrum of displacements of sounded volume; curves *1* and *2* are estimates obtained from numerical simulation with the data sampling frequency $\Delta t^{-1} = U/\Delta x$ and $\Delta t^{-1} = U/a_0$, respectively; the dashed curve is calculation by Eq. (13).

Analysis of the results of simulation shows that the probability density of displacements of the sounded volume z_{max} is close to the Gaussian one. Thus, using the spectrum (13) and the calculated results on σ_z^2 (see Figs. 2 and 3), we can simulate random realizations of $z_{max}(t)$ over the spectral range, omitting simulation of propagation of the sounding beam through the turbulent atmosphere.

2.2. Time spectrum of wind velocity measured by lidar

To calculate the spectrum of the wind velocity measured by lidar $S_D(f) = 2 \int\limits_{-\infty}^{+\infty} d\tau \, \langle V_D(t+\tau) \, V_D(t) \rangle \, e^{-2\pi j f \tau}$, it is necessary, according to Eq. (1), to simulate the

radial velocity $V_r(z, t)$ along with simulation of $Q_s(z, t)$ when determining $V_D(t)$. Random realizations of $V_r(z, t)$ were simulated in the spectral range based on the Karman model[10] for the one-dimensional spatial spectrum $S_V(\kappa_z)$. The Karman model included two parameters: the variance σ_V^2 and the integral correlation scale L_V of wind velocity. On the assumption of isotropic turbulence, from $S_V(\kappa_z)$ we can readily obtain the two-dimensional spatial spectrum $S_V(\kappa_z, \kappa_x)$ and, using the hypothesis of frozen turbulence, pass from the simulated realization $V_r(z, x)$ to $V_r(z, t)$ ($x = Ut$). The results presented below were obtained for $\sigma_V = 1$ m/s and $L_V = 50$ m.

Using the data of numerical simulation for $V_D(t)$, the spectra $S_D(f)$ were calculated. Figure 7 shows the spectra $S_D(f)$ at $R = 500$ m and different values of the mean velocity U (curves *1*, *2*, and *3* correspond to $U = 1$ m/s; curves *4*, *5*, and *6* correspond to $U = 4$ m/s) and C_n^2 (curves *1* and *4* are for $C_n^2 = 0$; curves *2* and *5* are for $C_n^2 = 10^{-14}$ m$^{-2/3}$; and curves *3* and *6* correspond to $C_n^2 = 10^{-13}$ m$^{-2/3}$). In the absence of fluctuations of the refractive index ($C_n^2 = 0$), the spectra $S_D(f)$ calculated using the data of numerical simulation agree well with calculations by Eq. (8), where $\varepsilon = 0.67\sigma_V^3/L_V$, in the high-frequency range. The results of calculations by this equation are shown in Fig. 7 as dashed curves.

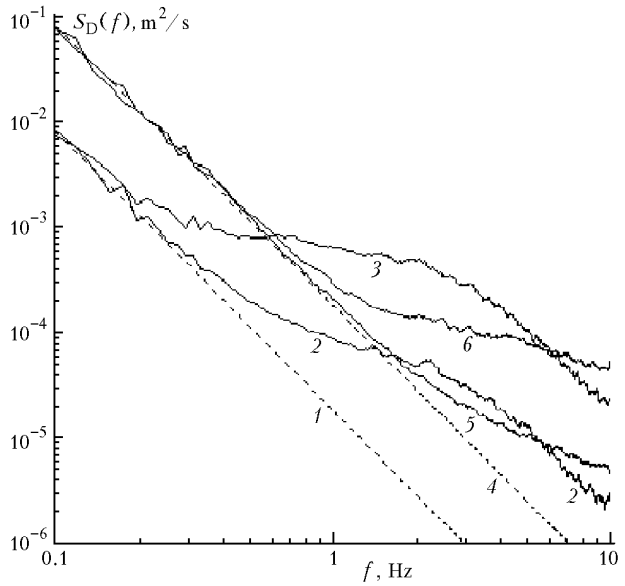

Fig. 7. Spectra of velocity estimated from data of Doppler lidar.

Averaging of the radial wind velocity over the sounded volume acts as a low-frequency filter of fluctuations of the measured velocity, and the spectrum $S_D(f)$ is proportional to $f^{-8/3}$ instead of $S_D(f) \sim f^{-5/3}$ corresponding to point-by-point measurements. Random displacements of the sounded volume $z_{max} - \langle z_{max} \rangle$ caused by turbulent fluctuations of the refractive index lead to extra spread in velocity estimates. Since the correlation time τ_z is comparable with the integral time t_0, random displacements of the sounded volume must finally cause the increase in fluctuations of the measured velocity at high frequencies in comparison with the case $C_n^2 = 0$. One can see from Fig. 7 that the increase of C_n^2 causes an essential increase of the energy of fluctuations in the high-frequency range of the spectrum $S_D(f)$.

Figure 8 shows the spectra $S_D(f)$ for the $C_n^2 = 10^{-13}$ m$^{-2/3}$, $U = 4$ m/s, and different R as solid curves. It is seen that the larger is R (and, according to Eq. (9), the longer is the sounded volume), the stronger is the effect of increase of the spectral density at the high frequencies. For $R = 250$ m the power dependence (8) for the spectrum $S_D(f)$ keeps up to the frequency $f \approx 1$ Hz (compare the solid and dashed curves *1*). For $R = 1$ km the frequency range, in which Eq. (8) is fulfilled, is considerably narrower: $f \approx 3$ Hz (compare the curves *3*). This should be necessarily taken into account when determining the dissipation rate of kinetic turbulence ε from lidar data based on Eq. (8). Narrowing of the frequency interval, within which ε is estimated, causes the increase in the error of its estimation.[11] It is clear that measurements of ε at $R = 250$ m are more accurate than at $R = 1$ km.

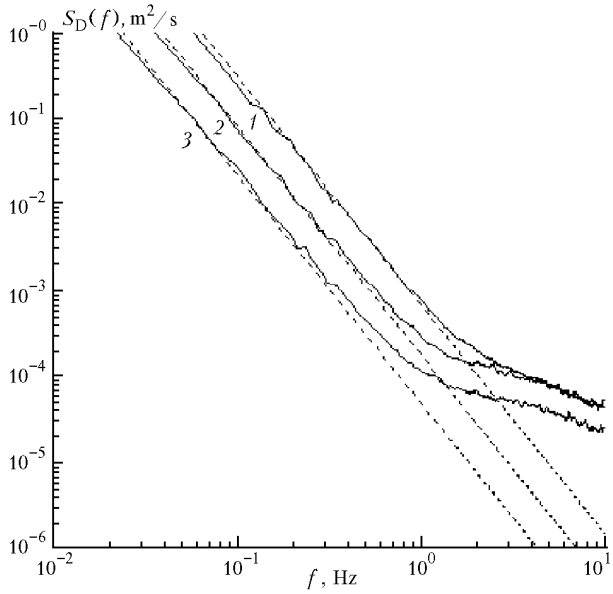

Fig. 8. Spectra of velocity estimated from Doppler lidar data simulated at $R = 250$ m (*1*), 500 m (*2*), and 1 km (*3*); $C_n^2 = 10^{-13}$ m$^{-2/3}$.

The effect of turbulent fluctuations of the refractive index on the spectrum $S_D(f)$ measured by the Doppler lidar depends on the wind velocity component U transverse to the beam axis. The higher is U, the stronger is averaging of random displacements of the sounded volume $z_{max} - \langle z_{max} \rangle$ for the time t_0 and the less essential is the effect of optical turbulence.

The data of Fig. 7 show that at weak wind $U = 1$ m/s (certainly, if the hypothesis of frozen turbulence is valid) it is impossible to estimate the dissipation rate of the turbulent energy using Eq. (8) even for relatively low turbulence $C_n^2 = 10^{-14}$ m$^{-2/3}$.

Conclusion

Using numerical simulation, we have studied the effect of turbulent fluctuations of the air refractive index in the atmosphere on the time spectrum of wind velocity measured by the cw Doppler lidar. For the lidar operating at the wavelength $\lambda = 10.6$ μm it has been shown that optical turbulence can cause essential random displacements of the sounded volume along the axis of propagation of the sounding beam. For example, for $C_n^2 = 10^{-13}$ m$^{-2/3}$ and $R = 1$ km the mean square deviation of longitudinal displacements of the center of the sounded volume is $\sigma_z \approx 50$ m. The correlation time of these displacements is approximately equal to the time of transfer of medium inhomogeneities by the cross wind to the distance equal to the initial radius of sounding beam.

The time spectra of velocity have been calculated for different levels of turbulence of the refractive index in the atmospheric surface layer. It has been found that random displacements of the sounded volume due to turbulence of the refractive index can lead to the essential increase in the energy of fluctuations in the high-frequency range of the turbulent spectrum of wind velocity measured by the cw Doppler lidar. A similar increase in the amplitude of the spectrum at high frequencies was observed in field experiments as well.

Acknowledgments

The work was partially supported by the Russian Foundation for Basic Research (Grant No. 98–05–03131–64033).

References

1. I.N. Smalikho, Atmos. Oceanic Opt. **8**, No. 10, 788–793 (1995).
2. V.A. Banakh, Ch. Werner, F. Köpp, and I.N. Smalikho, Atmos. Oceanic Opt. **10**, No. 3, (1997).
3. V.A. Banakh, I.N. Smalikho, F. Köpp, and Ch. Werner, J. Atmos. Oceanic Technol. **16**, No. 7, 1044–1061 (1997).
4. V.A. Banakh, I.N. Smalikho, and Ch. Werner, Appl. Opt., to be published (2000).
5. T.R. Lawrence, D.J. Wilson, C.E. Craver, I.P. Jones, R.M. Huffaker, and J.A. Tomson, Rev. Sci. Instrum. **43**, No. 3, 512–518 (1972).
6. I.L. Lumley and H.A. Panofsky, *The Structure of Atmospheric Turbulence* (Interscience, New York, 1964).
7. A.S. Monin and A.M. Yaglom, *Statistical Fluid Mechanics* Part 2 (Nauka, Moscow, 1967), Part 2, 720 pp.
8. V.P. Kandidov, Usp. Fiz. Nauk **166**, No. 12, 1309–1338 (1996).
9. N.L. Byzova, V.N.Ivanov, and E.K.Garger, *Turbulence in Atmospheric Boundary Layer* (Gidrometeoizdat, Leningrad, 1989), 263 pp.
10. N.K. Vinnichenko, N.Z. Pinus, S.M. Shmeter, and G.N. Shur, *Turbulence in the Free Atmosphere* (Gidrometeoizdat, Leningrad, 1976), 287 pp.
11. I.N. Smalikho, Atmos. Oceanic Opt. **10**, No. 8, 559–563 (1997).